Ultramicroscopy: PDF for review

Journal	Ultramicroscopy
Article ID	ULTRAM_265
Title	STROBOSCOPIC IMAGE CAPTURE: REDUCING THE DOSE PER FRAME BY A FACTOR OF 30 DOES NOT PREVENT BEAM-INDUCED SPECIMEN MOVEMENT IN PARAFFIN
Version	2
Article type	Full-length article
Submitted	21 Dec 05

Files submitted

Name	Fig No	Format	Use	Description
Fig1rev.tif	1	Figures (TIFF)	Maybe	
Fig2rev.tif	2	Figures (TIFF)	Maybe	
Fig3rev.tif	3	Figures (TIFF)	Maybe	
Fig4rev.tif	4	Figures (TIFF)	Maybe	
Fig5rev.tif	5	Figures (TIFF)	Maybe	
Fig6rev.tif	6	Figures (TIFF)	Maybe	
Fig7rev.tif	7	Figures (TIFF)	Maybe	
FinalTypke.STROBO_IMAGE.doc		Manuscript (Microsoft Word)		

Figure No: 1

Legend:

Figure 1

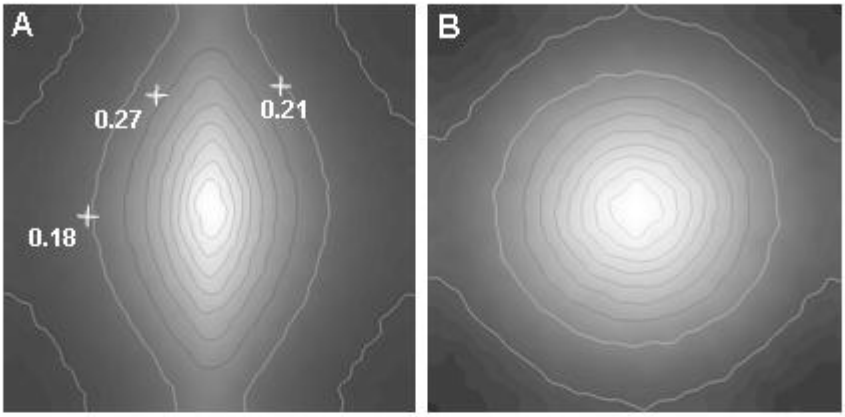

Figure No: 2

Legend:

Figure 2

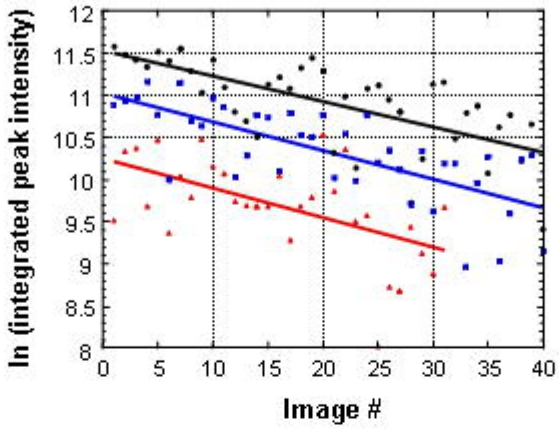

Figure No: 3

Legend:

Figure 3

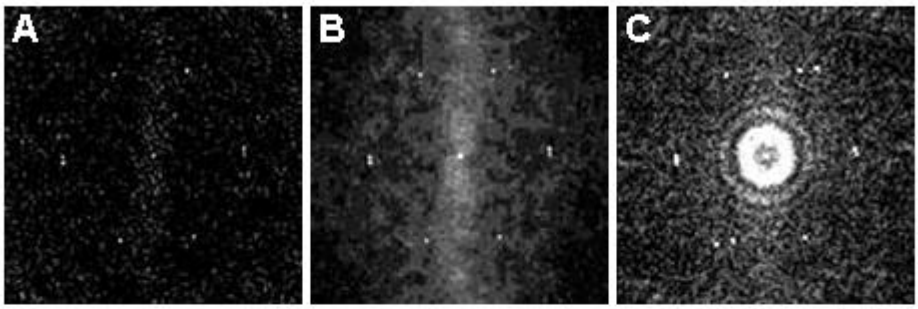

Figure No: 4

Legend:

Figure 4 Displacement maps

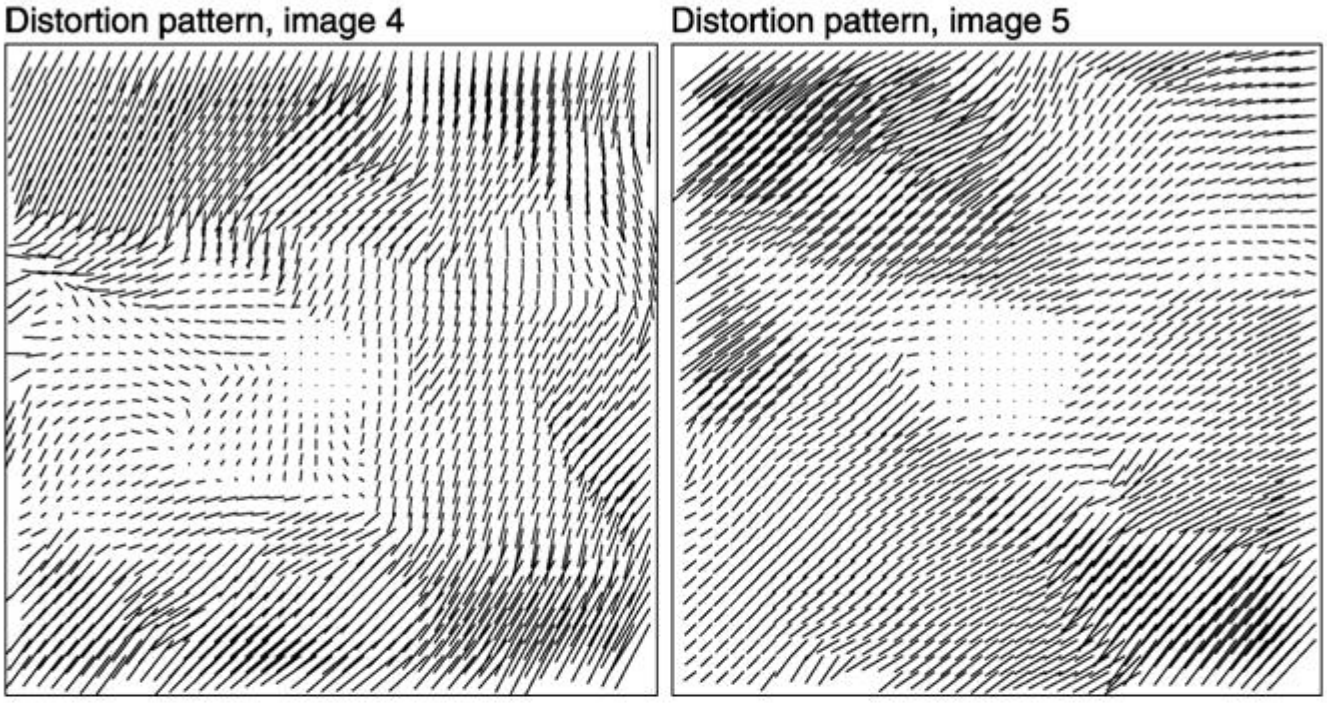

Figure No: 5

Legend:

Figure 5

A

image 4 before unbend

20	50	5	44	15	38	17
37	23	57	24	50	47	40
54	23	110	46	40	88	15
70	86	118	131	76	35	28
78	88	93	109	86	18	23
55	41	33	61	22	15	76
20	41	58	64	93	51	17

image 5 before unbend

52	42	9	71	104	56	56
86	72	85	98	53	40	36
29	24	42	64	68	29	11
62	87	142	115	55	42	38
95	73	48	130	49	33	24
11	41	3	79	100	32	61
34	38	56	51	51	24	31

B

image 4 with pattern 4

23	8	13	9	26	23	44
16	31	10	15	38	7	30
29	6	19	13	14	28	31
48	70	114	296	95	73	2
23	24	15	18	21	23	24
3	28	21	24	19	12	25
30	34	2	30	8	6	38

image 5 with pattern 4

20	60	54	33	34	28	7
44	34	13	36	29	53	2
51	23	35	53	15	43	41
34	97	42	133	52	1	16
7	24	32	18	29	11	6
24	13	24	13	3	19	23
22	8	29	45	64	45	9

C

image 4 with pattern 5

52	55	26	39	22	13	7
21	40	35	21	14	63	47
14	11	20	15	17	38	29
21	15	73	139	109	20	42
36	32	28	13	13	7	61
72	26	37	20	42	16	45
5	53	15	50	42	32	42

image 5 with pattern 5

20	32	18	28	20	2	17
30	22	16	16	33	43	16
17	15	18	17	15	26	38
66	103	133	249	96	34	20
8	19	15	5	33	6	30
29	21	29	8	23	33	15
64	14	28	17	15	30	27

Figure No: 6

Legend:

Figure 6

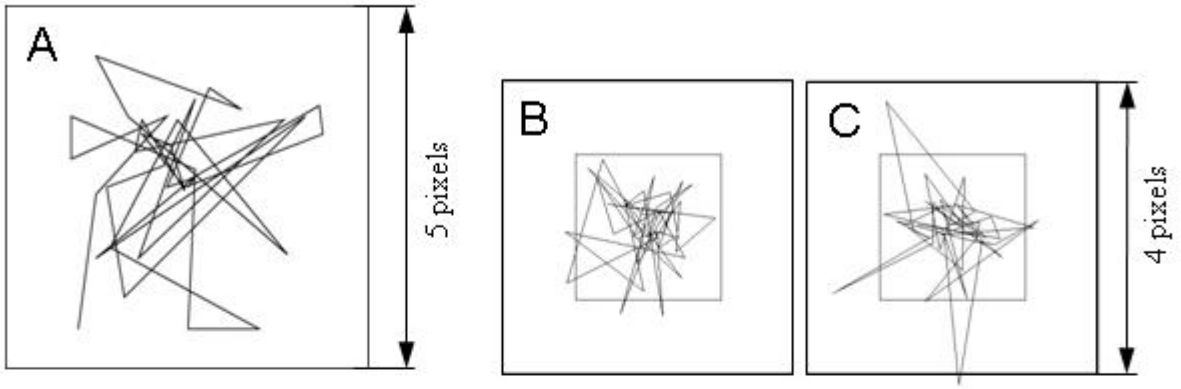

Figure No: 7

Legend:

Figure 7

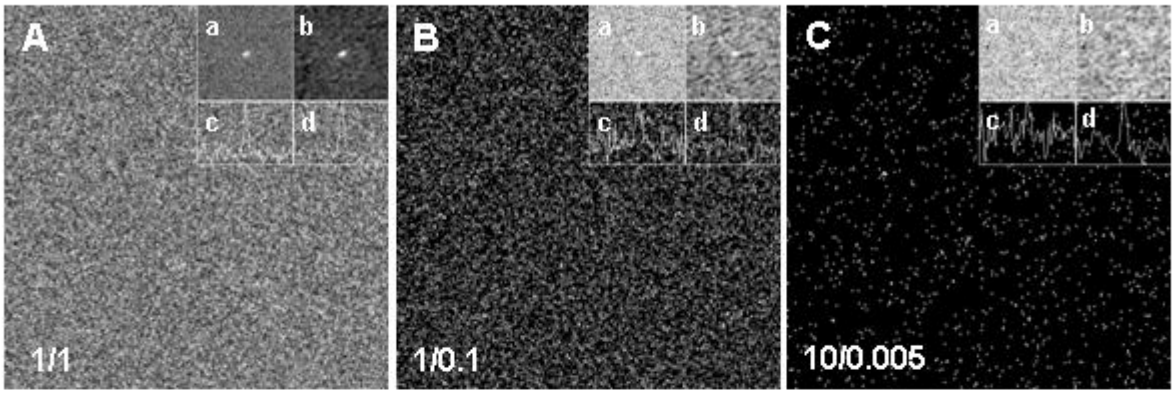

Revised May 22, 2006

STROBOSCOPIC IMAGE CAPTURE: REDUCING THE DOSE PER FRAME BY A FACTOR OF 30 DOES NOT PREVENT BEAM-INDUCED SPECIMEN MOVEMENT IN PARAFFIN

Dieter Typke[1], Christopher J. Gilpin[2], Kenneth H. Downing[1], and Robert M. Glaeser[1,3 *]

[1]Life Sciences Division, Lawrence Berkeley National Laboratory, Berkeley, CA 94720

[2]Department of Cell Biology, University of Texas Southwestern Medical Center, Dallas, TX 75390

[3]Department of Molecular and Cell Biology, University of California, Berkeley, CA 94720

Key words:
Stroboscopic image capture, beam-induced specimen movement, high dynamic range CCD camera, paraffin, electron microscopy

corresponding author:
Robert M. Glaeser
Donner Laboratory
Lawrence Berkeley National Laboratory
Berkeley, CA 94720
Tel: 510-642-2905
Fax: 510-486-6488
e-mail: rmglaeser@lbl.gov

ABSTRACT

Beam-induced specimen movement may be the major factor that limits the quality of high-resolution images of organic specimens. One of the possible measures to improve the situation that was proposed by Henderson and Glaeser (Henderson and Glaeser, 1985), which we refer to here as "stroboscopic image capture", is to divide the normal exposure into many successive frames, thus reducing the amount of electron exposure – and possibly the amount of beam-induced movement – per frame. The frames would then be aligned and summed. We have performed preliminary experiments on stroboscopic imaging using a 200-kV electron microscope that was equipped with a high dynamic range CCD camera for image recording and a liquid N_2-cooled cryoholder. Single-layer paraffin crystals on carbon film were used as a test specimen. The ratio F(g)/F(0) of paraffin reflections, calculated from the images, serves as our criterion for the image quality. In the series that were evaluated, no significant improvement of the $F_{image}(g)/F_{image}(0)$ ratio was found, even though the electron exposure per frame was reduced by a factor of 30. A frame-to-frame analysis of image distortions showed that considerable beam-induced movement had still occurred during each frame. In addition, the paraffin crystal lattice was observed to move relative to the supporting carbon film, a fact that cannot be explained as being an electron-optical effect caused by specimen charging. We conclude that a significant further reduction of the dose per frame (than was possible with this CCD detector) will be needed in order to test whether the frame-to-frame changes ultimately become small enough for stroboscopic image capture to show its potential.

INTRODUCTION

Beam-induced specimen movement, which may be caused by various factors such as specimen charging, structural rearrangements of the supporting film under the beam, instabilities of the ice or other embedment surrounding the specimen and beam-damage processes to the specimen itself, severely limit the success rate of recording high-resolution data of biological macromolecules with the electron microscope. Quite a number of different measures to improve the situation have been suggested and tried (Bullough and Henderson, 1987; Downing and Glaeser, 1986; Henderson and Glaeser, 1985; Typke et al., 2004).

One of the proposed methods, for which we now use the term "stroboscopic image capture", divides the exposure that is normally used to record an image into a large number of sub-exposures (Henderson and Glaeser, 1985). In the ideal case, images that are recorded with a fraction of $1/n^{th}$ of the full exposure would experience only $1/n^{th}$ of the beam-induced movement per frame. The effect of beam-induced movement should then be at least partially reduced after computational alignment and summation of the fractional-dose images. The reduction in electron exposure is limited, however, by the requirement that alignment of the frames by cross-correlation (CC) must be possible. If the signal-to-noise ratio would not be sufficient to distinguish the correct correlation peak in the cross-correlation function (CCF) between pairs of low-dose images, one could use a high-dose image recorded at the end of the series for aligning the low-dose frames in order to extend the degree of dose-fractionation that can be used.

Recent progress in CCD camera development makes it possible to consider fractionating the dose in this way. Recording stroboscopic image series on photographic film or on older-type CCD cameras is impractical at exposures that are significantly less than is normally used with beam-sensitive specimens, due to the low signal-to-noise ratio of these recording media at low electron exposures. More recently, however, high-dynamic range CCD cameras have become available, which provide a significantly higher signal-to-noise ratio at low exposures. For instance, for the camera that was used for the experiments described in this paper, the conversion rate was measured as about 165 counts per electron, while the root mean square (rms) background noise was less than 6 counts.

Here we describe first experiments on stroboscopic image capture with such a high-dynamic range CCD camera, using single-layer paraffin crystals on carbon film as a test specimen. As is documented below, the paraffin crystals exhibited rather strong movements even when the

exposure per frame was as low as 32 e^-/nm^2, which is about $1/30^{th}$ the exposure usually applied to record a high-resolution image of this kind of sample. This result suggests that the regime in which stroboscopic image capture would become effective for such specimens would first commence at even smaller doses per frame. We show by simulation that image alignment can be performed successfully at even lower exposures than used here. The relatively slow readout of present-day CCDs will then be a limitation, because when recording a stroboscopic image series, the equivalent of a single image would take several minutes. Very likely this limitation will be overcome by a new generation of pixel detectors (Faruqi et al., 2003).

MATERIALS AND METHODS

Electron microscopy

The experiments were carried out on a JEM 2100F electron microscope (JEOL, Tokyo, Japan) that was equipped with a field emission gun and a F224HD CCD camera (TVIPS, Gauting, Germany). The microscope was operated at 200 kV accelerating voltage, and the specimen was cooled to -180 ^{0}C using a liquid-nitrogen cooled cryoholder (Gatan, Pleasanton, California, USA). As the normal spot-size settings of the microscope did not allow for very low dose rates, the free lens-control option of the microscope was used to set the C1 condenser to its maximum current. In this way sufficiently low dose rates for the fractionated exposures could be achieved. The CCD camera can be set at two different modes, designated as the “high capacity” and the “low noise” modes, respectively. For the present studies it was operated in the “low noise” mode, in which it has a very high signal-to-noise ratio. The pixel size of this CCD camera is 24 μm.

Paraffin test specimens were prepared on holey carbon film that was covered with a thin carbon film as described (Typke et al., 2004). Before applying the paraffin solution, the carbon-coated grids were heated to ca. 1000 ^{0}C under high vacuum for 15 minutes, in order to enhance the conductivity of the carbon film and to stabilize its structure.

A number of stroboscopic image series were recorded with doses per frame in the range of 30 to 200 e^-/nm^2. Most of the series were recorded in form of 1024x1024 images, using the central part of the CCD without binning of pixels, in order to reduce the time per frame. When data were collected in this mode, a beam blanker (above the specimen) was used to limit the exposure time per frame to as little as 200 ms, and the readout time per frame was about 4 s. Specimen drift was

therefore negligible during the exposure of individual frames, but successive frames had to be aligned due to the long time that was required to collect a full stroboscopic image series.

Quantitative evaluation of image-contrast

As in previous work (Henderson and Glaeser, 1985; Typke et al., 2004), the amplitude ratio $F_{image}(g)/F_{image}(0)$ of paraffin reflections was used to characterize the image quality. For evaluating the images the EM and MRC software packages (Hegerl, 1996; Crowther et al., 1996) were used. The amplitudes $F_{image}(g)$ of the paraffin reflections were calculated in two different ways. Using the EM system software on the raw images, the amplitudes were computed as the square root of the intensity integrated over a 5x5 pixel area centered at the respective peak of the power spectrum, from which the background, determined in a 21x21 pixel area surrounding the peak, had been subtracted. With the MRC software, amplitudes were computed after correcting for image distortions as a vector sum over the 2x2 pixels nearest the reciprocal point, and the background was determined from the perimeter of a 7x7 box surrounding the spot. The spot amplitudes $F_{image}(g)$ were corrected for the MTF of the CCD camera before computing $F_{image}(g)/F_{image}(0)$ ratios. The CTF of the microscope was assumed to be close to 1 for the best images, and no correction was made for the envelope of the CTF and other instrumental imperfections.

Performance of the CCD camera

The linearity of the CCD and the response time of the microscope beam blanker were checked from an exposure series, with exposure times ranging from 1 ms up to 500 ms. As expected, excellent linearity was found (De Ruijter, 1995). The response time of the EM shutter was found to be 7 ms. The sensitivity of the CCD was determined as 165 ADU ("analog-digital units" or counts) per primary electron, relying on the current density measurement of the microscope. Images without electron exposure had an rms deviation of about 6, which means that the mean signal-to-noise ratio of electron events is about 27. Integrated single-electron signals, evaluated from images with extremely low exposure, were found to cover a wide range from about 100 to 500 counts, which is in reasonable agreement with the sensitivity that was measured.

Single-electron signals were found to be streaked at very low exposures. This streaky behavior disappeared at higher exposures. Because of the streaks of single-electron signals, however, the modulation transfer function (MTF) of the CCD depends strongly on the exposure. In order to determine the damping of spatial frequencies by the MTF, a uniformly exposed frame was used that was recorded with about 0.6 electrons per pixel, about the lowest exposure used for a single frame in a stroboscopic image series. Figure1A shows a two-dimensional representation of the "apparent MTF", calculated as the square root of the smoothed power spectrum. Due to the streaked single-electron signals at this exposure, the MTF decreases much faster in the x- than in the y-direction. The asymmetry of the MTF becomes even more pronounced at lower exposures, but disappears at exposures above about 5 electrons per pixel. The crosses in Fig. 1A mark positions of paraffin reflections that were recorded in one image series and the numbers are the corresponding values of the apparent MTF.

It should be mentioned that the streaks in the electron readout of the CCD can be avoided by optimal filter adjustment for extremely low signals, a procedure that must be done in the factory (H. Tietz, personal communication). For comparison Fig.1B shows the apparent MTF of such an optimized camera at an extremely low exposure of only 0.01 electrons per pixel for 100 kV electrons (I. Daberkow, personal communication). The improved MTF demonstrated in Fig. 1B shows promise for using such a detector to extend stroboscopic imaging to lower exposures than reported here.

Alignment of individual stroboscopic image-frames

In order to align the frames, a central peak that was due to the correlation of the common background structure imposed by the flat/dark correction had to be eliminated from the CCF before the correct peak indicating the specimen displacement between the frames could be detected. In some cases the correct peak was weaker than some of the background peaks. Even in these cases the correct peak could be identified by calculating the CCF not only for neighboring frames but also for frames that were farther apart in the sequence of frames. After aligning and summing up several frames, the sum image was used as a new reference. For the final alignment, images 11 to 20 were aligned with respect to the sum image '1 through 10', and all other images were aligned with respect to the sum image '11 1through 20', thereby ensuring that the frame to be aligned was not included in the average that was used as the reference. The alignment of the

two sum images, '1 through 10' and '11 through 20', was found to be within 0.01 pixel. The accuracy of alignment of a single frame is expected to be within 0.2 pixels, as has been verified by image simulations (see the final section of this paper). The aligned frames were added up and the F(g)/F(0) ratio was determined.

RESULTS

Fading of diffraction intensities shows normal behavior during a stroboscopic exposure series

One particular image series, for which we have carried out an extensive and detailed analysis, consisted of 40 successive frames recorded by using just the 1024x1024 pixels within the central area of the CCD camera. The electron exposure in this series was 32 e^-/nm^2 for each frame, the lowest value that is practical to use with this particular camera. The nominal microscope magnification was 120,000x (192,000x on the CCD), resulting in a pixel size, referred to the specimen, of 0.125 nm. The objective lens defocus of 400 nm (underfocus) in this series produces a CTF for the microscope that has a maximum close to the spatial frequencies of the first three paraffin reflections, two of which are at the spatial frequency $(0.41nm)^{-1}$ and the third at $(0.37nm)^{-1}$.

In spite of the low electron exposure per frame that was used in this series, four to five pairs of diffraction spots (corresponding to two overlaid monolayer crystals) can be recognized in the calculated power spectra of all frames. As mentioned above, the ratio $F_{image}(g)/F_{image}(0)$ calculated from the Fourier transform of the images was used to evaluate the image quality (Henderson and Glaeser, 1985; Typke et al., 2004). For some of the early frames in this series, values of $F_{image}(g)/F_{image}(0)$ up to about 0.016 were observed, which is 8% of the theoretically expected value of $F_{image}(g)/F_{image}(0)$ at 200 keV for the 0.41 nm reflections. About the same values had been found without the use of stroboscopic imaging (Typke et al., 2004). Thus, the ratio $F_{image}(g)/F_{image}(0)$ of single stroboscopic frames did not show a clear improvement compared to good images recorded on holey carbon film using a dose of about 1,000 e^-/nm^2.

In Figure 2, the integrated spot intensities of the two 0.41 nm reflections and the 0.37 nm reflection from one of the crystal lattices are shown in a logarithmic representation as a function of the image number. Although the intensities vary considerably from frame to frame, these variations are no greater than what is expected from electron statistics, according to image simulations that we performed (data not shown). The frame-to-frame variations in spot

intensities should thus not be taken as an indication of beam-induced specimen movement. On average, there is a steady decrease of the intensity of each reflection. Straight lines fit to the data of each reflection correspond to an exponential decrease in which the spot intensity fades to a value that is 1/e of the initial intensity after a "characteristic dose," D_e, of about 1000 e^-/nm^2. This is essentially in agreement with other measurements of the decay of electron diffraction intensities of organic materials at liquid nitrogen temperature (Brink and Chiu, 1990).

The sum of image frames and the sum of their power spectra behave as expected

Individual frames in a stroboscopic series can be aligned by cross correlation (CC). Accurate alignment of successive frames was possible solely on the basis of the granular phase contrast of the carbon film, with the diffraction spots from the paraffin lattice masked out. Judging from results obtained with simulations, the alignment error is expected to be less than 0.1 pixel, even though the electron exposure for each successive frame is only 0.3 e^-/nm^2. Successful alignment of frames recorded with such a low electron exposure was facilitated by the relatively high defocus of 400 nm.

As a further test that successive frames could be aligned accurately, we confirmed that the $F_{image}(g)/F_{image}(0)$ ratio of the coherent sum of all frames was equal to the value expected if one were to sum the same image, without imposing any movement, after first adjusting the Fourier amplitude for each successive "frame" to account for the exponential decay observed in figure 2. The experimental agreement, shown in table 1, verifies that errors in the alignment of individual frames did not cause a significant loss of signal, confirming that the alignment was effectively perfect in spite of the extremely low dose used per frame. As a further control, we also compared the sum of the power spectra of the individual frames to the value expected from the exponential decay. Single frames contribute differently to both sums; the weight of the earlier images is higher in the sum of diffraction patterns than in the sum of the images.

Figure 3 shows power spectra obtained from this series: (A) calculated power spectrum of the very first frame, (B) sum of all 40 power spectra, (C) power spectrum of the sum of all images after alignment by CC. Note that the coherent sum of all images displays Thon rings, which are much less visible in the sum of all power spectra.

Images of the paraffin crystal show marked beam-induced deformation from frame to frame

To test whether the stroboscopic images contain time-varying distortions that could be corrected computationally, lattice unbending (Henderson et al., 1986) was applied to the set of 40 frames. The first symmetry-allowed diffraction spots were treated as if they were the (1,0) and (0,1) spots of a pseudohexagonal, but actually monoclinic, lattice. Each paraffin chain thus fills an identical "pseudo" unit cell in this treatment. The unbending operation was applied after all frames had been aligned, as is described above, on the basis of the phase-contrast granularity of the carbon film.

Briefly, a filtered image was first produced by using a mask with about 5 pixels radius around each of the diffraction spots. A small section in the center of this filtered image, typically containing 200 - 500 unit cells, was used as a motif, which was cross-correlated with the raw image to search for positions of all unit cells within the original image. A vector displacement map, which indicates the shift in unit cell locations relative to those of an ideal lattice, was then used to define a function by which the image is interpolated back onto the ideal lattice.

In a subsequent refinement cycle, one of the unbent images was used to produce a new motif containing 200 unit cells with improved signal-to-noise ratio (SNR). This motif was then used in unbending each of the original images so that the lattice was shifted to the same origin in all of the images.

As expected, the diffraction spots became sharper after unbending, and as a result the signal in the most intense pixels increased to values that are about 10 times the noise in surrounding pixels. However, the $F_{image}(g)/F_{image}(0)$ ratio of the unbent images did not improve, indicating that all of the power from the signal was contained in the 5x5-pixel area of the transform used to compute $F_{image}(g)$ from the raw images.

The vector-displacement maps generated during the first step of unbending show that each stroboscopic frame is distorted in a unique way. Examples of the maps produced for two successive frames are shown in figure 4. The limited correspondence between the displacement maps implies that considerable movement within the irradiated area of the paraffin crystal occurs from one frame to the next. The implication of this observation is that beam-induced distortion of the paraffin crystal must, in fact, occur continuously over the period that each frame is being recorded.

Although unbending the images on the basis of these vector displacement maps has great value in reducing long-range disorder (and thus sharpening the computed diffraction spots), such

displays do not represent an absolute map of the vector displacements. An offset by an integral number unit cells can occur as the correlation-peak search algorithm passes from one region of well-defined peaks to another, across an area where peaks are not well defined. The exact path that the search algorithm follows across these less-defined areas also has a strong effect on how the regions of well-defined peaks appear to be organized into "domains". The result is that the vector displacement map may change somewhat when the search starts from different points. In spite of these limitations in such displays, the variations in the boundaries with well and poorly defined correlation peaks are seen to change from one frame to the next. This fact clearly indicates that considerable beam-induced motion occurs for exposures as low as 32 e^-/nm^2.

To confirm the point that each frame is distorted in a unique way, several of the frames were "unbent" using distortion patterns from other frames of the series. In all cases it was found that an unbending function which sharpened the diffraction spots for its own frame broadened the spots and weakened the amplitudes of other frames. Figure 5 illustrates this effect, showing the amplitudes extracted from the surroundings of one diffraction spot in transforms of the two frames shown in figure 4, (A) before unbending, (B,C) after unbending using the correct distortion pattern and after unbending using the distortion pattern determined for the other image. Note that in the latter case the strongest amplitude in the display of the transform is just as large as in the transform of the raw image, but the amplitude in adjacent pixels is now indistinguishable from the noise, due to broadening of the diffraction spot after an inappropriate "unbending" function has been applied to the image.

Exposure to the electron beam causes the paraffin specimen to move relative to the carbon film

We observed that the phases of the diffraction spots for the unbent images were random through the series, even though the carbon film components of the images were aligned to an accuracy corresponding to a small fraction of a unit cell. This observation suggests that the phase origin of the paraffin lattice moves from frame to frame, relative to a fixed point on the carbon film.

When the unbent images were aligned to a common phase origin by using the same motif in unbending, the phases of the diffraction spots were essentially the same for all frames, with a standard deviation of 5.4 degrees. However, in the Fourier transform of the coherent sum of the unbent images (i.e., after alignment to a common phase origin), the Thon rings from the

amorphous carbon support film are no longer as visible as they are in figure 3C. Apparently correcting the images so that the paraffin lattice is aligned has misaligned at least a portion of the carbon-film component of the images. One possible interpretation of this observation is that the carbon film does not experience the same distortion as does the paraffin crystal – in other words, the paraffin crystal moves relative to the carbon support film.

Alternatively, the weakening of Thon rings could be essentially an artifact of the unbending procedure. The correlation peak search procedure inevitably jumps by a poorly defined distance as it moves through areas where the correlation is weak. When the lattice is again picked up, the assigned vector displacement may be off from the true displacement by one unit cell or more. In effect, the assigned vector displacements may be correct, in effect, modulo one unit cell.

In order to confirm that the paraffin lattice does move with respect to the carbon, we looked at how the location of the unit cell closest to the center of the image moved from one frame to the next, bearing in mind that all images had been previously centered by CC of the image of the amorphous carbon. We are not able to say whether the positions of the unit cell that is closest to a fixed point of the carbon film are the true positions of the same unit cell, or whether the true position is the observed position plus one or more additional unit cells. The most conservative interpretation, of course, is to assume that the true position of the paraffin lattice has involved the smallest possible movement that is consistent with the data.

As is shown in figure 6A, the conservative estimate of the movement of the paraffin crystal relative to the carbon support film executes a random walk in which the frame-to-frame steps are typically about 2 pixels (i.e., about 0.25 nm). The length of these steps is significantly greater than the experimental error in the alignment of the carbon-film component of the images.

The fact that the paraffin lattice moves relative to the carbon film does not exclude the possibility that the carbon film itself also experiences beam-induced movement. To evaluate whether the carbon film contributes to the total effect of beam-induced movement, 256x256 pixel sub-areas at the center and the corners of the images of each of the aligned frames were cross-correlated with the coherent sum of all images. Two examples of the series of displacements that were found for successive frames are shown in figures 6B and C. In this case the displacements were found to be typically smaller than 1 pixel. As a consequence, this result indicates that the paraffin lattice not only experiences beam-induced movement relative to the carbon substrate, but that the underlying carbon film itself also undergoes structural

displacements, from frame to frame, that are smaller than those of the paraffin lattice. It was checked by simulation that these displacements are clearly greater than can be explained by electron statistics.

DISCUSSION

The original aim of these experiments was to find out whether stroboscopic image capture would make it possible to improve image contrast (signal). The basic concept was to computationally correct for incremental amounts of beam-induced movement that would otherwise accumulate over the course of a normal, low-dose electron exposure. The results of these experiments indicate, however, that the sought-for "stroboscopic" regime, if it even exists, has not yet been reached at exposures down to about 30 e^-/nm^2. On the contrary, we have observed that beam-induced movement is undiminished even at electron exposures that are about $1/30^{th}$ the dose normally used to record a high-resolution image of radiation-sensitive organic specimens.

It has been known for over 20 years that beam-induced movement causes a severe loss of contrast (measured as the F(g)/F(0) ratio) at high resolution for radiation-sensitive specimens (Henderson and Glaeser, 1985). It has been difficult to say, however, whether this effect is due primarily to specimen movement or image movement (which might result from beam-induced charging).

That some degree of beam-induced specimen movement occurs is not in question. Bend contours are easily seen to move over the course of low electron exposures if samples are relatively thick, although this is not usually seen in monolayer crystals. In addition, at least in the case of paraffin crystals, both wrinkling (Brink and Chiu, 1990) and bulging of the irradiated area (Downing, 1988) have been demonstrated to occur at high electron exposures. Dorset and Zemlin (1987) argued that an initial increase in diffraction intensity at low exposures indicated that paraffin chains were moving into more perfect alignment with the incident electron beam. Specimen charging, observed in the form of the Berriman effect (Downing et al., 2004; Glaeser and Downing, 2004), is also certain to occur in non-conducting materials such as paraffin crystals, even when they are supported on a well-conducting substrate.

We now report that a significant amount of movement occurs between the images of the paraffin crystal lattice and the images of the underlying carbon support-film. This relative movement of the two could not be caused by any electron-optical effect. These observations

therefore establish that physical movement of the specimen is a significant factor in reducing the image contrast at high resolution.

We believe that it is likely that the observed beam-induced movement is caused by mechanical stress that accumulates when products of radiolysis are generated that no longer fit into the molecular envelope of the original structure. In the case of paraffin the predominant form of damage appears to be the introduction of *trans* double bonds (Patel, 1975; Patel and Keller, 1975), which clearly results in a molecular shape that no longer fits into the original crystal lattice. In a more general situation, such as proteins and other biological materials, ionization will lead primarily to bond rupture, and as a result two atoms that previously were about 0.15 nm apart will separate to a distance of about 0.35 nm. This picture of radiolysis products that are not commensurate in size or shape with the cavity occupied by the parent molecule has been put forward earlier by McBride to explain the high pressure generated in an organic crystal after only 5 percent of the parent molecules have been cleaved by photolysis (McBride et al., 1986). It is even plausible that beam-induced reconfiguration of carbon-carbon bonds occurs in the apparently stable "amorphous carbon" support film, and the resulting stresses generated in that way cause the support film itself to also undergo beam-induced movement. The pressure observed by McBride to build up in a three-dimensional crystal, about half of that required to convert graphite to diamond, would likely be relieved well before that point by processes such as expansion, slippage, and buckling in the case of a thin-foil specimen.

It remains unclear at this point whether the principle of recording images as a series of frames taken with even lower exposures could still prove to be helpful. The first question in this regard would be whether images could still be aligned if the electron exposures were reduced by another order of magnitude. The question of alignment of images is addressed in the final section of this paper, where it is shown that one must align the frames by using a statistically well-defined reference image if they are recorded with exposures that are lower than those already investigated here. For exposures that are lower by about a factor of 10, a properly tuned CCD camera will still be suitable. For even lower exposures the frames would have to be recorded with a detector that operates as a digital counter (Faruqi et al., 2003; Milazzo et al., 2005) in order to avoid the noise associated with a broad pulse-height spectrum for the individual electron events.

CROSS-CORRELATION OF SIMULATED LOW-DOSE IMAGES

Although we determined that the signal-to-noise (S/N) ratio of the peak in the cross-correlation function (CCF) between a single frame and the sum of 10 aligned frames (from which the single frame was excluded) was approximately 10, a relatively high value, we still needed to evaluate how accurate the alignment is likely to be for such a value of the S/N ratio. In order to make such an estimate, we prepared stochastic representations, generated as a Poisson process, of the nearly noise-free image produced by alignment and averaging of all 40 frames. A modulation transfer function similar to the experimental one shown in figure 1 was then used to simulate the down-weighting of high-resolution information about the location of individual electron events that occurs in real experimental data. Stochastic versions of this image that were sufficiently noisy to produce a peak in the CCF with a S/N = 10 were then found to be aligned with an accuracy of at least 0.2 pixels. Interestingly, to produce stochastic representations of the starting image that yielded a peak in the CCF with a S/N as low as 10, the simulated electron exposure had to be 0.05 electron/pixel, a factor of 10 lower than our single, experimental image-frames. We believe that it is likely that effectively random, beam-induced movement of the carbon film similar to that indicated in figure 6, which was not modeled in these simulations, may be a major factor that caused the S/N to be much smaller in the experimental images than it was in the simulations. In any case, the important point is that the accuracy in the simulated alignment was evaluated at the same value of the S/N ratio for the peak in the CCF.

Analytic theory for the signal-to-noise ratio of the cross-correlation peak

In order to address the question of how far the number of electrons per frame can be reduced without losing the ability to align the frames, we carried out further numerical simulations and compared the results that were obtained with what is to be expected from theory. For the cross-correlation (CC) of two bright-field images that display small density variations, a formula for the signal-to-noise ratio, P, of the CC peak depending on the signal-to-noise ratio, p, of the image elements and the number, M, of independent image elements has been derived (Hoppe and Hegerl, 1980) (see also (Saxton, 1978):

$$P = \sqrt{\mathrm{M}}\, p^2 \Big/ \sqrt{2p^2 + 1}\,. \qquad (1a)$$

The signal-to-noise ratio p of the image elements may be expressed as $p = \rho / \sigma$, where ρ is the root mean square signal contrast of the image, and σ is the noise contrast of the image, which

according to Poisson statistics is given by $\sigma = \mathrm{N}^{-1/2}$, with N being the number of electrons per pixel. Note that the number M of independent image elements is normally smaller than the number of pixels, e.g. due to the fall-off of the MTF at higher frequencies. When the images have been recorded with different doses and therefore the signal-to-noise ratios of the image elements are different for the two images, the formula takes the form

$$P = \mathrm{g}\sqrt{\mathrm{M}}\,\frac{p_1 p_2}{\sqrt{1 + {p_1}^2 + {p_2}^2}}, \qquad (1b)$$

where p_1 and p_2 are the signal-to-noise ratios of the image elements of the two images, respectively. An additional factor g has been introduced in equation (1b) to account for degradations of the correlation peak, e.g. due to radiation damage or slight relative rotations. In the simulation we identify M with the number of pixels; then the factor g also reflects the loss of signal due to the fall-off of the power spectrum due to the MTF of the detector.

We discuss two special cases:

a) Cross-correlation of a well-defined image with a noisy one ($p_1 >> 1;\ p_2 << 1$):

$$P = g\sqrt{\mathrm{M}}\,p_2. \qquad (2)$$

In order to find the correct correlation peak, one generally requires $P \geq 5$, which leads to $p_2 \geq 5/g\sqrt{\mathrm{M}}$, and a minimum number of electrons per pixel in the second image of $\mathrm{N}_2 \geq 25/\mathrm{g}^2\mathrm{M}\rho^2$. The minimum number of electrons per pixel is thus inversely proportional to the mean square image contrast and the number of pixels. For example, for a 1024x1024 image area, $g = 1$ and the signal contrast $\rho = 0.1$, the number of electrons per pixel has to be $\mathrm{N}_2 \geq 2.4 \cdot 10^{-3}$, which means that one electron in 420 pixels would still give a distinguishable CC peak if one image is well-defined. On the other hand, the signal contrast may be as low as 0.022 when the low-dose image is recorded with 1 electron per 20 pixels, i.e. with a ten-fold lower dose than the images of the series that was evaluated in the previous paragraphs.

b) Cross-correlation of two noisy images ($p_1 << 1;\ p_2 << 1$):

$$P = g\sqrt{\mathrm{M}}\,p_1 p_2. \qquad (3)$$

Requiring $P \geq 5$ leads to $p_1 p_2 \geq 5/g\sqrt{M}$, and $N_1 N_2 \geq 25/g^2 M\rho^4$. In the example with $M = 1024^2$, $g = 1$, and $\rho = 0.1$, the condition to be fulfilled is $N_1 N_2 \geq 0.24$. If both images have the same exposure, i.e. $N_1 = N_2 = N$, the condition becomes $N \geq 0.5$ for $\rho = 0.1$.

For the comparison of the results of the simulation with theoretical values obtained from equations (1a) or (1b), we should remark that they are in principle slightly different. In equations (1a) or (1b), the signal-to-noise ratios *P* of the peak refer to ensemble averages, while in the simulation we compare the CC peak with the rms variation of the CCF outside the peak. The difference is an additional term $p_1^2 p_2^2$ in the square root of the denominator of equation (1b). This term can, however, be neglected for the cases we are interested in.

Numerical simulations agree with the analytical theory

In order to be close to a real situation, we used a micrograph of carbon film covered with a single-layer paraffin crystal for the simulations. The image had been recorded on film at 400 keV accelerating voltage, a magnification of 60,000, and about 300 nm underfocus, using an electron exposure of about 1000 electrons per nm^2. The micrograph was scanned in a Nikon Super Coolscan 8000 ED scanner with 6.35 μm pixel size (0.106 nm pixel size at the specimen), and the output was converted to optical density. A 1024x1024-pixel area was extracted from the digitized image, and the image contrast was arbitrarily adjusted to 10%. Due to the low dose, the image was too noisy to see Thon rings in its power spectrum. This reference image was considered to be structural information for the purpose of our numerical simulations. Images with different exposures were generated by distributing electrons according to Poisson statistics, with the expected values of each pixel being proportional to the signal in the reference image.

The results of the simulations are summarized in Table 2. There is a good overall agreement between theory and simulation. The correct correlation peak was found in the simulation as long as P_{calc} was greater than about 5. Close to this limit, peaks in the background of the CCF were sometimes found to be higher than the correct CC peak. When the CC peak is not well defined, it may be worthwhile to calculate a "double CCF" meaning the cross-correlation of the CCF that was determined in the first step with a well-defined CC peak. This correlation of the CCF with a well-defined peak makes use of the surroundings of the peak and is therefore expected to improve the reliability of the peak search (Kirkland et al., 1995; Typke and Dierksen, 1995).

Values of the signal-to-noise ratio, $P'_{simulation}$, of the double CCF are listed in the last column of the table. For low exposures these peaks are in fact better defined than the usual CC peaks.

It is astonishing to see that the correlation still works when the first image is well-defined ($N_1 = \infty$) but only about 1 electron in 300 pixels is used to record the second image (last line of the first block). When the number of electrons per pixel is the same in both images, the lowest dose for the CC to work is – for the given contrast value of 0.1 – about 0.5 electrons per pixel. This is about the dose at which the image series investigated in this work was recorded. For three examples, Figure 7 shows one quarter of one of the correlated images with inserts showing (a) the central part of the CCF, (b) central section through the CCF, (c) the central part of the double CCF, i.e. the CCF between the field in (a) and a well-defined CCF peak determined by cross-correlating two well-defined images, (d) central section through the function shown in (c).

The results of these simulations suggest that it should be possible to align stroboscopic image frames that are recorded with an electron exposure that is 100 times lower than what has been used in the current experiments. Such experiments will require the use of a detector that is essentially noise-free and has a DQE close to 1, however. It is important that such experiments be carried out in order to determine whether the expected regime can be reached in which the amount of beam-induced movement of the specimen is a small fraction of what still occurs for exposures as small as 30 electrons/nm^2.

Abbreviations:

ADU = Analog-Digital Units (same as 'counts', digital output values of the CCD camera)

CCD = Charge-Coupled Device

CC = Cross-Correlation

CCF = Cross-Correlation Function

CTF = (Phase) Contrast Transfer Function

MTF = Modulation Transfer Function

Acknowledgements

This work was supported by NIH grant GM51487, and by the Director, Office of Science, Office of Basic Energy Sciences, of the U.S. Department of Energy under Contract No. DE-AC02-05CH11231.

References

Brink, J., andW. Chiu. 1990. Analysis of image contrast in high-resolution images of *n*-paraffin at 400 kV and -167°C. *In* Proc. XIIth Int'l. Cong. Electron Microsc. Peachey LD, Williams DB, editors. San Francisco Press, Inc., Seattle, WA. 86-87.

Bullough, P., andR. Henderson. 1987. Use of spot-scan procedure for recording low-dose micrographs of beam-sensitive specimens. *Ultramicroscopy* 21(3):223.

Crowther, R.A., R. Henderson, andJ.M. Smith. 1996. MRC Image Processing Programs. *Journal of Structural Biology* 116(1):9.

De Ruijter, W.J. 1995. Imaging properties and applications of slow-scan charge-coupled device cameras suitable for electron microscopy. *Micron* 26(3):247.

Dorset, D.L., andF. Zemlin. 1987. Specimen movement in electron-irradiated paraffin crystals -- A model for initial beam damage. *Ultramicroscopy* 21(3):263.

Downing, K.H. 1988. Observations of restricted beam-induced specimen motion with small-spot illumination. *Ultramicroscopy* 24(4):387.

Downing, K.H., andR.M. Glaeser. 1986. Improvement in high resolution image quality of radiation-sensitive specimens achieved with reduced spot size of the electron beam. *Ultramicroscopy* 20(3):269.

Downing, K.H., M.R. McCartney, andR.M. Glaeser. 2004. Experimental characterization and mitigation of specimen charging on thin films with one conducting layer. *Microscopy and Microanalysis* 10:790-796.

Faruqi, A.R., D.M. Cattermole, R. Henderson, B. Mikulec, andC. Raeburn. 2003. Evaluation of a hybrid pixel detector for electron microscopy. *Ultramicroscopy* 94(3-4):263-276.

Glaeser, R.M., andK.H. Downing. 2004. Specimen charging on thin films with one conducting layer: discussion of physical principles. *Microscopy and Microanalysis* 10:783-789.

Hegerl, R. 1996. The EM Program Package: A Platform for Image Processing in Biological Electron Microscopy. *Journal of Structural Biology* 116(1):30.

Henderson, R., J.M. Baldwin, K.H. Downing, J. Lepault, andF. Zemlin. 1986. Structure of purple membrane from halobacterium halobium: recording, measurement and evaluation of electron micrographs at 3.5 A resolution. *Ultramicroscopy* 19(2):147.

Henderson, R., andR.M. Glaeser. 1985. Quantitative analysis of image contrast in electron micrographs of beam-sensitive crystals. *Ultramicroscopy* 16:139-150.

Hoppe, W., andR. Hegerl. 1980. Three-dimensional structure determination by electron microscopy (nonperiodic specimens). Hawkes PW, editor. Springer-Verlag, Berlin, Heidelberg, New York.

Kirkland, A.I., W.O. Saxton, K.L. Chau, K. Tsuno, andM. Kawasaki. 1995. Super-resolution by aperture synthesis: tilt series reconstruction in CTEM. *Ultramicroscopy* 57(4):355.

Milazzo, A.-C., P. Leblanc, F. Duttweiler, L. Jin, J.C. Bouwer, S. Peltier, M. Ellisman, F. Bieser, H.S. Matis, andH. Wieman. 2005. Active pixel sensor array as a detector for electron microscopy. *Ultramicroscopy* 104(2):152.

Patel, G.N. 1975. Crystallinity and the effect of ionizing radiation in polyethylene. V. Distribution of trans-vinylene and trans,trans conjugated double bonds in linear polyethylene. *Journal of Polymer Science: Polymer Physics Edition* 13(2):351 - 359.

Patel, G.N., andA. Keller. 1975. Crystallinity and the effect of ionizing radiation in polyethylene. II. Crosslinking in chain-folded single crystals. *Journal of Polymer Science: Polymer Physics Edition* 13(2):323 - 331.

Saxton, W.O. 1978. Computer Techniques for Image Processing in Electron Microscopy. Marton L, Marton C, editors. Academic Press, New York.

Typke, D., andK. Dierksen. 1995. Determination of image aberrations in high-resolution electron microscopy using diffractogram and cross-correlation methods. *Optik* 99:155-166.

Typke, D., K. Downing, andR. Glaeser. 2004. Electron microscopy of biological macromolecules: Bridging the gap between what physics allows and what we currently can get. *Microscopy and Microanalysis* 10:21-27.

Figure and Table Legends

Fig. 1. Smoothed amplitude spectra of images recorded with uniform illumination, which provide estimates of the apparent modulation transfer function (MTF) for two different TVIPS F 224 HD CCD cameras. (A) Apparent MTF of the CCD camera used in these experiments at 200 kV accelerating voltage and an exposure of 0.6 electrons per pixel. The crosses indicate the positions of paraffin reflections, and the associated numbers are the respective values of the apparent MTF of the evaluated image series. (B) Apparent MTF of an optimized CCD camera obtained at 100 kV accelerating voltage and only 0.01 electrons per pixel. The MTFs are contoured at values of 0.1, 0.2, etc.

Fig. 2. Spot intensities of three reflections (integrated over 5x5 pixels in the power spectrum) of one of the paraffin crystals, plotted on a logarithmic scale against the image number. The strong variations of the amplitudes within the series cannot be taken as indications of beam-induced movements, because they may be caused by statistical fluctuations.

Fig. 3. (A) Power spectrum of the first frame of a stroboscopic series of images, (B) sum of all 40 power spectra, (C) power spectrum of the coherent sum of all images.

Fig. 4. Unbending functions for images 4 (left) and 5 (right). The maps show the local movements required to shift unit cells of the paraffin crystal onto a regular lattice. Displacement vectors are drawn with a length 3 times the actual displacement.

Fig. 5. Amplitudes near the (1,1) diffraction spot in Fourier transforms of (A) the raw images 4 and 5 (left and right, respectively), (B) the same images, after unbending using the distortion pattern determined for image 4, and (C) the same images, after unbending using the distortion pattern determined for image 5.

Fig. 6. Movements of features in the series of aligned images. As was mentioned earlier in the text, the images were treated as if each paraffin chain corresponded to one unit cell of a monoclinic (nearly hexagonal) lattice. As a result, the unit cell referred to in panel A is actually a “pseudo” unit cell. Figure 5A shows the location of the unit cell closest to the center of the

image. The width of the plot is 5 pixels, corresponding to 0.62 nm. The line indicates the movement with respect to the center of the sum image, from frame to frame, which appears to have no preferred direction. Figure 5B and C show the movement of two areas of the carbon film, 256 pixels on edge. The first area was located at the center of the frame and the second area was located at the lower left corner of the frame. The width of these plots is 4 pixels, or 0.5 nm, and it is seen that the carbon-film component of the specimen moves far less than does the paraffin lattice. It was checked by image simulation that the displacements found for the extracts of the carbon film are not artifacts due simply to electron statistics. According to this simulation, displacements of extracts from the same positions as above that are due to electron statistics were within 0.12 pixels.

Fig. 7. Cross-correlation of simulated images of a pattern with image contrast ρ = 0.1, with different numbers of electrons. (A) Both images simulated with 1 electron per pixel; (B) Both images simulated with 0.1 electrons per pixel; (C) First image with 10, the second with 0.005 electrons per pixel. Only one quarter of the images is shown. In order to make single electrons signals visible, they are displayed as 3x3 pixel spots. See the text for an explanation of the insets in the upper right corner of the images.

Table 1. Image quality relative to that of an ideal image for a stroboscopic image series. $F_{diffraction}(g)$ and $F_{diffraction}(0)$ are amplitudes measured in electron diffraction patterns for the scattered and unscattered beams. $F_{image}(g)$ and $F_{image}(0)$ are amplitudes measured in the Fourier transforms of the images.

Table 2. Signal-to-noise ratios $P_{simulation}$ of the cross-correlation peak, and $P'_{simulation}$ of the double cross-correlation peak, of simulated images depending on the number of electrons per pixel. The factor g of formula (1b) is assumed to be 1.

Table 1: Image quality relative to that of an ideal image for a stroboscopic image series.

	$\frac{F_{image}(g)/ F_{image}(0)}{2 F_{diffraction}(g)/ F_{diffraction}(0)}$							
reflections	frame 1	frame 20	frame 40	Coherent sum image expected	found	Sum of power spectra expected	found	Critical dose D_e [e^-/nm^2]
0.41 nm #1	0.065	0.055	0.032	0.034	0.033	0.042	0.048	1,000
0.41 nm #2	0.071	0.066	0.030	0.044	0.044	0.046	0.055	1,000
0.37 nm	0.031	0.052	0.020	0.028	0.024	0.030	0.033	1,000

Table 2. Signal-to-noise ratios $P_{simulation}$ of the cross-correlation peak and $P'_{simulation}$ of the double cross-correlation peak of simulated images depending on the number of electrons per pixel. The factor g of formula (1b) is assumed to be 1.

N_1	N_2	p_1	p_2	$P_{simulation}$	P_{theor}	$P'_{simulation}$
∞	0.1	∞	0.032	31.8	32.4	28.2
∞	0.01	∞	0.01	10.4	10.2	9.5
∞	0.003	∞	0.0055	6.4	5.6	5.4
10	1	0.32	0.1	29.7	30.7	34.1
10	0.1	0.32	0.032	9.9	9.8	13.2
10	0.03	0.32	0.017	5.3	5.3	8.4
1	1	0.1	0.1	8.4	10.1	16.5
1	0.3	0.1	0.055	6.6	5.6	10.4
0.5	0.5	0.071	0.071	6.2	5.1	9.4